ACS APPLIED ENERGY MATERIALS

www.acsaem.org Article

Efficient Charge Transfer and Carrier Extraction in All-Polymer Solar Cells Using an Acceptor Filler

Fang-Chi Hsu,* Jin-Wen Luo, Yu-Wei Su, Cheng-Syun Yang, Yu-An Lin, Jia-Yu Lin, Chi-Yuan Chang, Yang-Fang Chen,* and Chi-Ping Li

Cite This: *ACS Appl. Energy Mater.* 2020, 3, 4217−4225 Read Online

ACCESS | Metrics & More | Article Recommendations | Supporting Information

ABSTRACT: All-polymer solar cells (all-PSCs) exhibit considerably improved mechanical and thermal stability than their polymer−fullerene counterparts. Despite their advantages, the power conversion efficiencies of all-PSCs are still lower than those of polymer−fullerene PSCs. In this study, we demonstrate that introducing a small amount of fullerene or non-fullerene acceptors as filler into the photoactive layer of PBDBT:N2200 all-PSCs can enhance charge transport properties and, thereby, the device performance. An appreciable enhancement (∼21%) in the power-conversion efficiencies (PCEs) of all-PSCs, from 6.13% to 7.42%, is obtained when fullerene with the amount of 25 wt % PBDBT is added. The performance improvement is primarily from the enhanced short circuit current density (J_{SC}), which can be attributed to the enhanced exciton dissociation, reduced charge recombination, and balanced charge transport in the prescence of the fullerene filler. Similar behavior is also observed when fullerene is replaced by ITIC molecules. Importantly, the fullerene filler shows a negiligible effect on the device storage and light-soaking stability. Therefore, all-PSCs incorporating a proper selected acceptor filler is an efficient way to improve device performance without sacrificing stability. We believe that our study can pave a useful approach for developing stable and high performance PSCs.

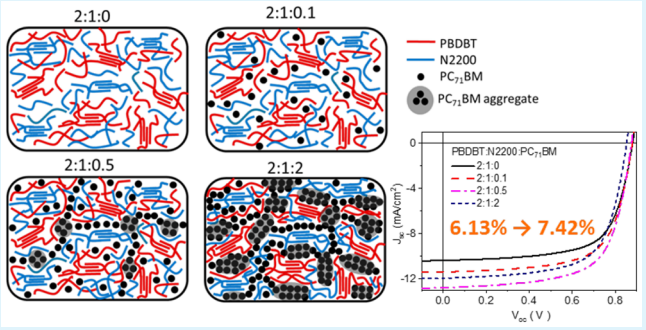

KEYWORDS: *charge extraction, charge transport, ternary, filler, all-polymer solar cell*

Downloaded via NATL TSING HUA UNIV on January 28, 2021 at 03:00:01 (UTC).
See https://pubs.acs.org/sharingguidelines for options on how to legitimately share published articles.

1. INTRODUCTION

Polymer solar cells (PSCs) have been considered as one of the most promising power generation technologies for flexible, wearable, and large area device applications due to their excellent features of mechanical properties, processing simplicity, semitransparency, and lightweight.[1−6] Typically, p-type polymers are intermixed with n-type acceptors, forming a bulk heterojunction structure as the photoactive material in response to incoming photons. Substantial efforts have been focused on using fullerene derivatives as acceptor intermixed with a variety of polymer donors for the development of fullerene-based PSCs, producing power conversion efficiency (PCE) over 10%.[7−11] Though fullerene and its derivatives are of high electron mobility, they are easy to aggregate, which leads to lower device stability. In contrast to fullerene-based acceptors, non-fullerene acceptors with a variety of chemical structures have been developed and the PCEs of corresponding solar cells can exceed more than 16%.[12] Moreover, those non-fullerene-based devices show a better stability than fullerene-based cells.[13−15] Recently, a specific type of PSCs, all-PSCs, utilizing n-type polymers as acceptors has gained considerable attention.[16,17] This combination exhibits remarkably improved mechanical and thermal stability in comparison with fullerene-based devices.[18,19] Generally, n-type polymers based on naphthalene diimide or perylene diimide moieties have been developed for high efficiency all-PSCs. A record PCE of 10.1% has also been achieved for single junction all-PSCs adopting naphthalene diimide moiety based poly{[*N*,*N*′-bis(2-octyldodecyl)naphthalene-1,4,5,8-bis(dicarboximide)-2,6-diyl]-*alt*-5,5′-(2,2′-bithiophene)} (N2200).[20]

To improve PCE of all-PSCs, commonly used approaches for fullerene-/non-fullerene-based PSCs, including solvent annealing[21] and solvent additive,[22] have been demonstrated to be effective. Recently, Xu et al.[23] have reported that introducing n-type molecular dopants into the photoactive layer can efficiently restrain charge recombination in all-PSCs, resulting in enhanced device performance. Ternary strategies offer further improvements in binary PSCs. Mostly, the incorporated third component is also either fullerene or small molecules for polymer−fullerene/−non-fullerene systems. Considering polymer−polymer systems, Li et al.[24] have

Received: November 26, 2019
Accepted: April 10, 2020
Published: April 10, 2020

© 2020 American Chemical Society

https://dx.doi.org/10.1021/acsaem.9b02302
ACS Appl. Energy Mater. 2020, 3, 4217−4225

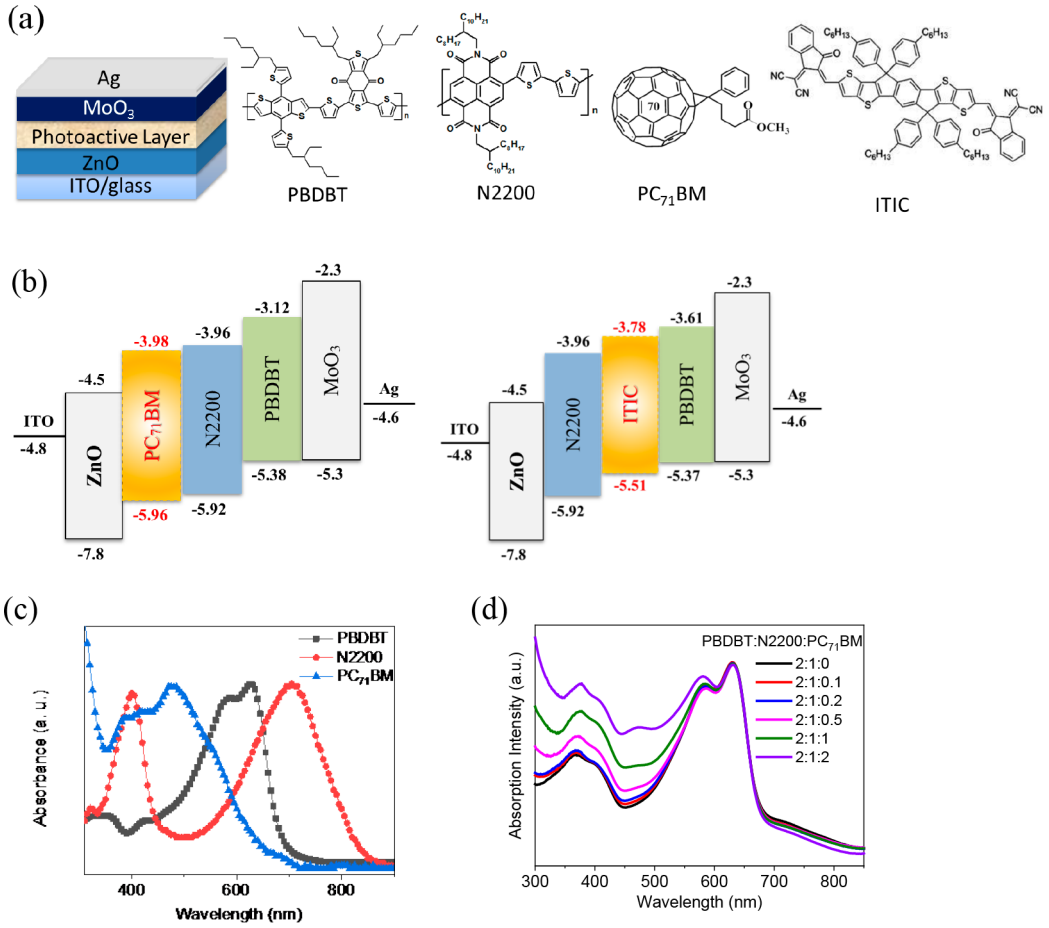

Figure 1. (a) Device structure of inverted all-PSCs and molecular structures of PBDBT, N2200, $PC_{71}BM$, and ITIC. (b) Schematic representation of energy levels in fabricated devices. (c) Normalized UV−vis absorption spectra of pure PBDBT, N2200, and $PC_{71}BM$ films. (d) Absorption spectra of blend films with various $PC_{71}BM$ contents.

shown that it is also effective by incorporating a second polymer donor based on the Förster resonant energy transfer mechanism. Lee et al.[25] have demonstrated ternary devices with optimal content of polymer:fullerene acceptor mixture for high mechanical and photovoltaic performances. Though the reported ternary devices show improved performance, those works mostly are based on tuning two-donor (or two-acceptor) fraction under an overall constant donor-to-acceptor (D/A) ratio. From the morphological perspective, typically, a semicrystalline polymer is composed of ordered and disordered phases. Disordered phase resulting from randomly oriented polymer chains is of lower density and contains free volume in contrast to the densely packed ordered phase. Despite the muture interaction between donor and acceptor polymers, there is still free volume residing in the resulting chain packing morphology on the microscopic level. The free volume opens up possibilities for charge manipulation.

To manipulate charges through the free volume, we introduce small molecules as filler into all-PSCs. In contrast to the conventional ternary system keeping the overall D/A ratio constant, in our study, various amounts of fillers are added into the all-polymer blend with a fixed D/A ratio resulting in a nonconventional ternary system. The concept of using the third component as filler in all-PSCs is rarely seen in the literature. We choose poly[(2,6-(4,8-bis(5-(2-ethylhexyl)-thiophen-2-yl)benzo[1,2-*b*:4,5-*b*′]dithiophene)-*co*-(1,3-di(5-thiophene-2-yl)-5,7-bis(2-ethylhexyl)benzo[1,2-*c*:4,5-*c*′]-dithiophene-4,8-dione)] (PBDBT) as the donor (D) polymer intermixed with the acceptor (A) polymer N2200 to serve as the binary model system. PBDBT:N2200 is one of the efficient all-polymer blends for non-fullerene solar cells.[11,25,26] The criteria for an active filler are as follows; (i) it should be of good charge transport properties, (ii) it should be compatible with polymer donors and acceptors to form favorable morphologies, and (iii) its energy levels should form a cascade band alignment structure with the host donor and acceptor. In our model system, the hole mobility is higher than the electron mobility.[22] Therefore, $PC_{71}BM$ and ITIC are selected as fillers and careful studies are performed in the blends containing $PC_{71}BM$. It is found that PCE of nonconventional ternary devices increases with $PC_{71}BM$ and ITIC loading. The advantages of using acceptor filler in all-polymer blend are providing an additional interface for exciton separation, reducing charge recombination probability, and forming an additional charge collection channel for its significant amount in acceptors. Beyond that, both the storage stability and the light-soaking stability of nonconventional ternary devices remain similar to filler-free all-PSCs.

2. EXPERIMENTAL SECTION

Material Preparation. ZnO sol−gel solution was prepared according to ref 27. Organic materials including PBDBT (Solarmer), N2200 (Polyera, M_n = 31.9 KD), and $PC_{71}BM$ (Lumtech.) were purchased commercially and used as received.

https://dx.doi.org/10.1021/acsaem.9b02302
ACS Appl. Energy Mater. 2020, 3, 4217−4225

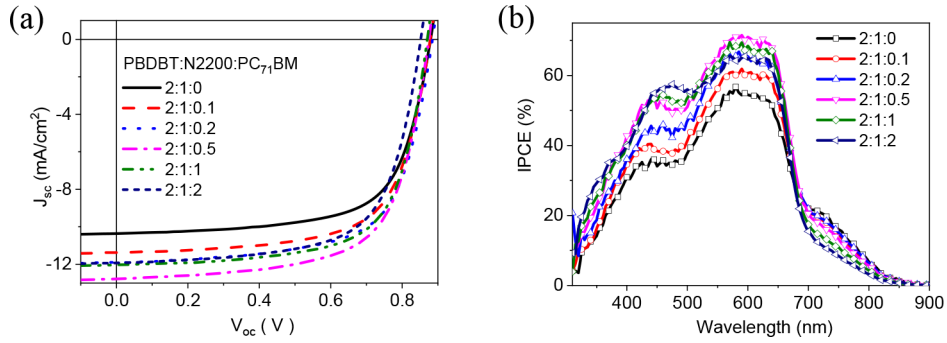

Figure 2. Performance of PBDBT:N2200:$PC_{71}BM$ devices with various amounts of $PC_{71}BM$. (a) $J-V$ characteristics. (b) IPCE spectra.

Table 1. Statistics and Best Photovoltaic Parameters of PBDBT:N2200:$PC_{71}BM$ Devices under 1 sun Condition with AM 1.5G Filter[a]

PBDBT:N2200:$PC_{71}BM$ (w/w/w)	J_{SC} (mA/cm^2)	V_{OC} (V)	FF (%)	PCE (%)	calcd J_{SC} (mA/cm^2)
2:1:0	10.29 ± 0.24(10.36)	0.88 ± 0.00 (0.88)	67.02 ± 0.83 (67.28)	6.06 ± 0.12 (6.13)	9.63
2:1:0.1	11.13 ± 0.20(11.37)	0.88 ± 0.00 (0.88)	66.12 ± 0.63 (67.05)	6.44 ± 0.13 (6.70)	10.42
2:1:0.2	11.70 ± 0.24(11.89)	0.88 ± 0.01 (0.89)	65.89 ± 0.94 (66.78)	6.71 ± 0.16 (7.03)	11.26
2:1:0.5	12.48 ± 0.19(12.78)	0.88 ± 0.00 (0.88)	66.10 ± 0.77 (66.33)	7.29 ± 0.06 (7.42)	12.17
2:1:1	11.99 ± 0.22(12.03)	0.87 ± 0.00 (0.87)	66.58 ± 0.75 (67.84)	6.91 ± 0.19 (7.11)	11.73
2:1:2	11.89 ± 0.16(11.92)	0.85 ± 0.00(0.85)	65.02 ± 0.57 (66.3)	6.56 ± 0.12 (6.74)	11.60
1:0:1	12.80 ± 0.10(12.83)	0.83 ± 0.00(0.83)	66.10 ± 0.37(66.59)	6.99 ± 0.07(7.08)	

[a]The values in the parentheses denote the values for the best device.

Sample Fabrication. Indium doped tin oxide (ITO) film with sheet resistance of 15 Ω/sq coated on glass substrate was served as the electrode. Those ITO glass substrates were cleaned by successive sonication in soap water, DI water, acetone, and ethanol followed by being dried under the nitrogen gas flow. Solar cells were fabricated on the basis of the inverted device structure of indium−tin oxide (ITO)/ZnO/photoactive layer/MoO_3/Ag. The electron transport layer ZnO in the thickness of 30 nm was deposited by spin-coating on the cleaned ITO substrates at 5000 rpm for 30 s followed by annealed at 180 °C in air for 1 h to remove the solvent. The photoactive layer was prepared by solubilizing PBDBT with N2200 in a fixed weight ratio of 2:1 in chlorobenzene with 0.5 vol % 1,8-diiodoctane for a total concentration of 12 mg mL^{-1}. $PC_{71}BM$ in amounts of 0, 0.4, 0.8, 2, 4, and 8 mg were added into the photoactive layer solution and stirred at 90 °C overnight before being used. The resulting weight ratios of PBDBT:N2200:$PC_{71}BM$ were 2:1:0, 2:1:0.1, 2:1:0.2, 2:1:0.5, 2:1:1, and 2:1:2. The optimized thickness of the photoactive layer is ∼90 nm, which was measured by a Veeco dektak 6 M surface profiler. Finally, a hole transport layer of MoO_3 (7 nm) and an anode electrode of silver (100 nm) were subsequently thermally deposited in order onto the photoactive layer at pressure below 2 × 10^{-6} Torr to complete the device fabrication. For the photoactive layer incorporating ITIC, ITIC of concentration of 2 mg mL^{-1} was added into PBDBT:N2200 solution. The subsequent device fabrication procedures were the same as those containing $PC_{71}BM$. The device working area defined by the overlapping of ITO and silver electrodes was 4 mm^2. Samples for AFM and optical measurements were of the same layered structures as solar cells without depositing MoO_3/Ag. The thicknesses of blend films were kept at ∼90 nm for performing the optical measurements. For Grazing-incidence wide-angle X-ray scattering (GIWAXS) and tunneling electron mocroscopy (TEM) studies, the photoactive films were prepared on silicon substrates. For TEM samples, those films on silicon substrates were then embedded in DI water after the films were dried. The films floated on the water surface were then collected on copper grids. Electron- and hole-only devices were fabricated using the configurations of ITO/ZnO/photoactive layer/Ca/Al and ITO/PEDOT:PSS/photoactive layer/MoO_3/Ag, respectively.

Characterization. The current density−voltage ($J-V$) characteristics of finished solar cells were evaluated by using a Keithley Model 2400 source meter under irradiation intensity of 100 mW/cm^2 from a calibrated solar simulator (Newport Inc.) with an AM 1.5G filter. The calibration was done by using a standard Si photodiode. The incident-photon-conversion-efficiency (IPCE) spectra were recorded using a setup consisted of a lamp system, a chopper, a monochromator, a lock-in amplifier, and a standard silicon photodetector (ENLI Technology). All of the measurements were conducted in the laboratory environment. Photoluminescence spectra were collected by a spectrometer (Fluorolog, Jobin Yvon). GIWAXS measurements were performed at the 23A beamline (10 keV) of the National Synchrotron Radiation Research Center (NSRRC), Hsinchu, Taiwan, using a 0.2° incident angle.

3. RESULTS AND DISCUSSION

Figure 1a illustrates the device configuration of fabricated all-PSCs along with molecular structures of the used materials (PBDBT, N2200, $PC_{71}BM$, and ITIC) in the photoactive layer. Figure 1b depicts the energy band diagrams of the studied devices. Those used materials form cascade band arrangement beneficial for carrier transport. Panels c and d of Figure 1 show the absorption spectra of pure materials and PBDBT:N2200 blends with various $PC_{71}BM$ contents. The absorption spectra of PBDBT and N2200 are well complementary with each other, spanning from UV to near-IR (NIR) regime (Figure 1c). In this study, the weight ratio of donor (D) PBDBT to primary acceptor (A_1) N2200 is kept at 2:1 in the photoactive layer for the best photovoltaic performance.[23,28,29] The content of the second acceptor (A_2) filler $PC_{71}BM$ with respect to N2200 is varied to optimize the D/A_1/A_2 (=2:1:A_2) ratio. Incorporating $PC_{71}BM$ into PBDBT:N2200 further enhances the photon absorption capability in the ultraviolet to visible regime (Figure 1d) and the enhancement increases with the increased $PC_{71}BM$ content.

Figure 2a presents the typical current density−voltage ($J-V$) characteristics of PBDBT:N2200 all-PSCs incorporated with various amounts of $PC_{71}BM$. The statistical results for the

https://dx.doi.org/10.1021/acsaem.9b02302
ACS Appl. Energy Mater. 2020, 3, 4217−4225

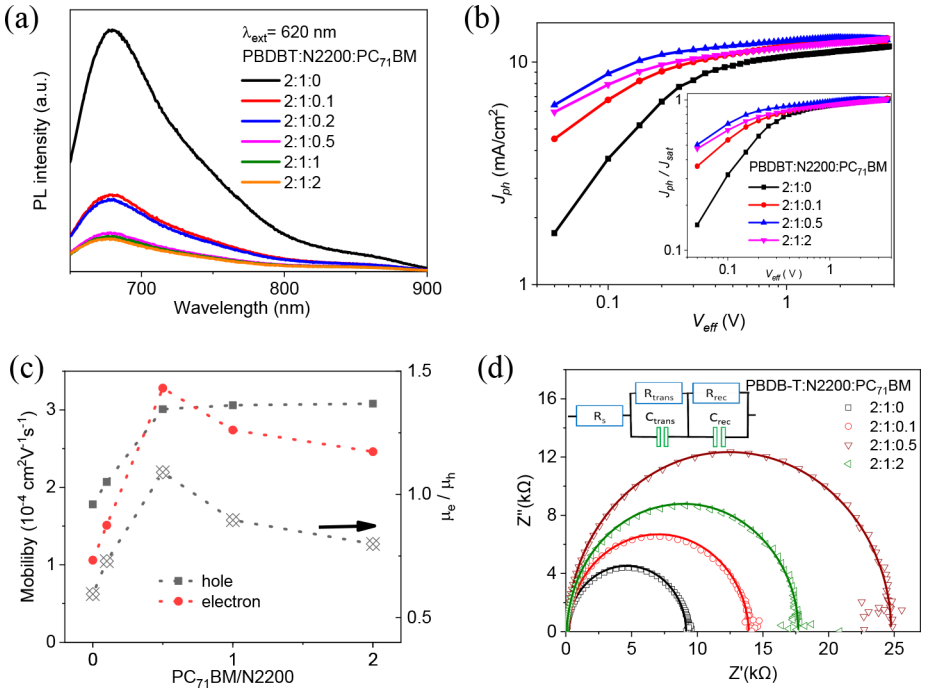

Figure 3. (a) PL spectra of blend films under 620 nm light excitation. (b) $J_{ph}-V_{eff}$ curves for PBDBT:N2200:$PC_{71}BM$ devices. (inset: $J_{ph}/J_{sat}-V_{eff}$ curves). (c) Hole (μ_h) and electron (μ_e) mobility of devices as well as electron-to-hole mobility ratio (μ_e/μ_h) based on various $PC_{71}BM$/N2200 weight fractions. (d) Nyquist plots of impedance spectra measured at the short circuit condition under 100 mW/cm^2 irradiation.

performance of each kind of devices over 20 cells are summarized in Table 1. The average PCE of the neat PBDBT:N2200 device (2:1:0) is 6.06%, a result which is similar to those reported in the literature.[23,28,29] Interestingly, PCE values increase with $PC_{71}BM$ contents and the optimal loading is at a blend ratio of 2:1:0.5, equivalent to 25 wt % PBDBT. The improvement of PCE primarily comes from the enhanced average short circuit current density (J_{SC}) from 10.29 to 12.48 mA/cm^2 leading to an enhanced average PCE of 7.29% from 6.06%, an ∼20.3% increment. For the champion device, a PCE value of 7.42% can be achieved, a result which is also better than PBDBT:$PC_{71}BM$ binary cell of optimal D/A ratio of 1:1 (see Table 1 and Supporting Information Figure S1 and Table S1). Therefore, the nonconventional PBDBT:N2200:$PC_{71}BM$ system has superior phovoltaic performance than the neat PBDBT:N2200 and PBDBT:PC_{71} BM ones.

The improvement of J_{SC} of the nonconventional ternary device is also confirmed by the IPCE spectra. As shown in Figure 2b, IPCE values enhance from 320 to 670 nm with adding $PC_{71}BM$ up to the optimal loading. Further increasing the loading of $PC_{71}BM$, IPCE values increase in the wavelengths shorter than 500 nm, whereas the responses of N2200 and PBDBT begin to decrease in the wavelength ranges of 650−800 and 500−650 nm, respectively. The result suggests that $PC_{71}BM$ can have significant contribution to the photon-to-charge conversion effect at much higher loading, and the reason will be discussed later. The calculated J_{SC} values from integrating the IPCEspectra are within 7% differences of those obtained from $J-V$ curves.

Though adding $PC_{71}BM$ into the PBDBT:N2200 system does significantly enhance the photon absorption capability of the all-polymer film, the improved photon flux does not strongly correlate with the enhancement of IPCE spectra. To gain more insight for J_{SC} improvement, charge transport properties, including exciton separation and carrier mobility, were studied to clarify the role of $PC_{71}BM$ in an all-polymer matrix. To understand the exciton dissociation processes of used materials, steady state photoluminescence (PL) spectra of pure and blend films were measured under 620 nm light excitation, as presented in Figure S2a and Figure 3a, respectively. Strong PL emission from PBDBT can be observed at 680 nm, whereas those from N2200 and $PC_{71}BM$ are relatively weak. The weak PL emission suggests that the excited electron prefers to return to the ground state through a rapid nonradiative process. Adding N2200 into PBDBT partly quenches the PL emission from PBDBT due to exciton dissociation at PBDBT/N2200 interfaces. The residual PL emission from the neat blend can be further quenched by the addition of $PC_{71}BM$, suggesting that PBDBT/$PC_{71}BM$ interfaces provide an additional route for exciton separation. For instance, ∼69% emission intensity was quenched at the 2:1:0.1 blend. At $D/A_1/A_2$ = 2:1:0.5, the PL quenching efficiency is nearly saturated. We have also tried to measure the PL emission of pure and blend films at excitation wavelength of 485 nm and obtained similar results (see Figure S2b,c). It is noted that PL emission of $PC_{71}BM$ strongly overlaps the absorption of N2200 (see Figure S2d), suggesting efficient energy transfer from $PC_{71}BM$ to N2200. On the other hand, we have also fabricated donor-free cells to determine charge transfer between N2200 and $PC_{71}BM$ in ternary blends. J_{SC} values of devices based on N2200 and $PC_{71}BM$ films are 0.009 and 0.101 mA/cm^2, respectively. Binary N2200:$PC_{71}BM$ devices with ratios of 1:0.5 and 1:2 show similar J_{SC} values of 0.095 and 0.092 mA/cm^2, respectively (see Figure S3). Obviously, the donor-free binary cells have J_{SC} value close to that of $PC_{71}BM$ device and much higher than that of the N2200 one, revealing that charge transfer between N2200 and $PC_{71}BM$ is possible but is not as efficient as devices based on regular p/n junctions of PBDBT/$PC_{71}BM$ and PBDBT/

https://dx.doi.org/10.1021/acsaem.9b02302
ACS Appl. Energy Mater. 2020, 3, 4217−4225

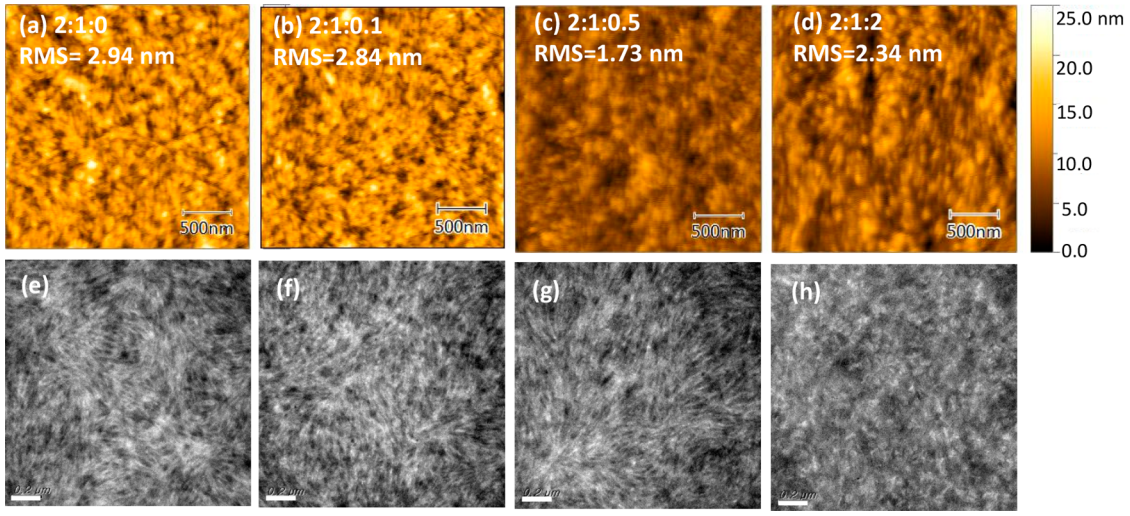

Figure 4. AFM height images (a–d) and corresponding SEM images (e–h) of different PBDBT:N2200:$PC_{71}BM$ ratios. The scale bar in TEM images is 0.2 μm.

N2200. Thus, the large PL quenching and energy transfer effect in the presence of $PC_{71}BM$ can contribute to J_{SC} improvement.

The contribution of photocarriers from PBDBT/$PC_{71}BM$ interfaces is also obtained from analyzing the photocurrent density–effective voltage ($J_{ph}-V_{eff}$) curves of PBDBT:N2200:$PC_{71}BM$ devices. Here, J_{ph} is defined as $J_{ph} = J_L - J_D$, where J_L and J_D are the current density under 1 sun light illumination and in the dark, respectively. V_{eff} is defined as $V_{eff} = V_0 - V_a$, where V_0 is the voltage when $J_{ph} = 0$ and V_a is the applied voltage. Generally, it is assumed that all photogenerated excitons can be separated into free charges at junction interfaces and then efficiently be collected by the individual electrode at high V_{eff}.[30,31] Accordingly, the saturation current density (J_{sat}) is dominated by the maximum exciton generation rate (G_{max}); i.e., $J_{sat} = qLG_{max}$, where q and L are the elementary charge and thickness of the photoactive layer, respectively. By analyzing the $J_{ph} - V_{eff}$ curves shown in Figure 3b, the G_{max} value is about 8.80×10^{27} m^{-3} s^{-1} for the champion nonconventional ternary PSCs, which is higher than 8.25×10^{27} m^{-3} s^{-1} for neat PBDBT:N2200 cells (see Table S2). The result indicates that photon harvesting of the nonconventional ternary films is more efficient in the presence of $PC_{71}BM$ filler. Since only a portion of excitons are separated into electrons and holes,[32] from the estimated G_{max}, the exciton dissociation efficiency, $P(E,T)$, can be determined by $J_{ph} = qLP(E,T)G_{max}$. By plotting the normalized photocurrent density (J_{ph}/J_{sat}) against V_{eff} to evaluate $P(E,T)$ (see the inset in Figure 3b), it clearly shows that the prepared ternary films do generate more free charges than the neat binary one, which verify their superior exciton quenching efficiency and charge generating ability. Under J_{SC} condition, the $P(E,T)$ values were calculated to be 91.85%, 93.40%, 96.90%, and 94.86% for 2:1:0, 2:1:0.1, 2:1:0.5, and 2:1:2 blends, respectively. The champion device has the most efficient exciton quenching and charge generating ability.

After exciton dissociation, the subsequent charge transport behavior in the continuous pathways formed by the constituent materials was studied by the space-charge-limited-current (SCLC) method. Both hole-only and electron-only device structures were fabricated, and the measured results are displayed in Figure S4. By using Mott–Gurney square law,[33] the calculated hole (μ_h) and electron mobilities (μ_e) for neat PBDBT:N2200 film were 1.78×10^{-4} and 1.06×10^{-4} cm^2 V^{-1} s^{-1}, respectively, which are similar to those reported in the literature.[34] After incorporating $PC_{71}BM$, μ_h rises progressively at first and then increases slowly, whereas μ_e rises rapidly initially and then decreases after reaching the optimal fullerene loading. The value of μ_e/μ_h increases at first and then decreases after passing the optimal fullerene content. The electron and hole mobilities are the most balanced at A_2/A_1($PC_{71}BM$/N2200) = 0.5, which correlates with the optimal device performance at the blend ratio of $D/A_1/A_2$ = 2:1:0.5 (see Figure 3c). The balanced charge transport property in the prepared ternary film may be one of the reasons for the high device performance compared to its PBDBT:N2200 binary cells.

On the other hand, charge recombination property at the interfaces is also important for charge collection. We performed impedance spectroscopy on those devices. Figure 3d illustrates the Nyquist plots of the impedance spectra for those devices in response to an ac perturbation of 50 mV varied over a frequency range from 100 to 2 MHz under short circuit condition and light irradiation at 100 mW cm^{-2}. The data were fitted to an equivalent circuit model[23] shown in the inset of Figure 3d. The intercept of the semicircle with the lateral axis at low frequency carries the information on the recombination resistance (R_{rec}).[35] The R_{rec} values obtained from each semicircle were 9.0, 13.8, 24.7, and 17.6 KΩ for 2:1:0, 2:1:0.1, 2:1:0.5, and 2:1:2 blends, respectively. As obtained, the higher R_{rec} of nonconventional ternary devices can help reduce the carrier loss across the photoactive films, wherein, in turn, more charges can be collected and lead to higher J_{SC}.

The variation of charge generation, recombination, and transport is very likely linked to the film morphology. Panels a–d of Figure 4 show the topographic images of different PBDBT:N2200:$PC_{71}BM$ ratios taken by atomic force microscopy (AFM). The corresponding root-mean-square (RMS) surface roughness values of those films were 2.94, 2.84, 1.73, and 2.34 nm for $D/A_1/A_2$ = 2:1:0, 2:1:0.1, 2:1:0.5, and 2:1:2, respectively. The incorporation of $PC_{71}BM$ smoothens the neat all-polymer film and the champion device has the smoothest photoactive layer. The result indicates that

https://dx.doi.org/10.1021/acsaem.9b02302
ACS Appl. Energy Mater. 2020, 3, 4217–4225

$PC_{71}BM$ can affect the mixing result of PBDBT:N2200 and the mixing of the champion blend is more homogeneous than the rest, an outcome which is also suggested by the TEM images. According to Figure 4e–g, the fibrillary structure can be clearly seen in the neat all-polymer film and the films with $PC_{71}BM$ loading up to A_2/A_1 = 0.5 due to the mutual interaction of PBDBT and N2200.[36,37] The 2:1:0.5 blend has the most homogeneous bright and dark field contrast. However, at weight ratio of 2:1:2, the film morphology changes from fibrous to granular structures, which may be due to a large amount of $PC_{71}BM$ interrupting the interaction between PBDBT and N2200.

To gain more insight into the microstructure change, we also compare the nanomorphology of those films using grazing-incidence wide-angle X-ray scattering (GIWAXS) (Figure S5). According to the 1D-GIWAXS linecut profile shown in Figure 5, q_{xy} and q_z denote the in-plane (dash line) and out-of-plane

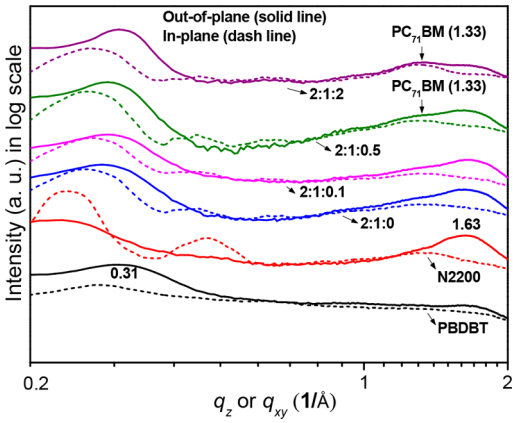

Figure 5. Linecuts of GIWAXS profiles along the out-of-plane and in-plane directions of pure PBDBT, pure N2200, and PBDBT:N2200:$PC_{71}BM$ photoactive layer films.

(solid line) components of the scattering vector **q**, respectively. The pure PBDBT film shows a pronounced (100) peak at q_z = 0.31 $Å^{-1}$ and a weak (100) peak at q_{xy} = 0.27 $Å^{-1}$, indicating the lamellar crystallites with a random or isotropic orientation as evidenced by the (100) ring, while the pure N2200 exhibits (100) and (200) peaks along the in-plane direction at 0.23 and 0.47 $Å^{-1}$, respectively, and a prominent (010) peak associated with $\pi-\pi$ stacking is located in the out-of-plane direction at q_z = 1.63 $Å^{-1}$. For the neat PBDBT:N2200 blend, the (100) peak of PBDBT in the out-of-plane direction shifts from 0.31 to 0.28 $Å^{-1}$, indicating the corresponding (100) lamellar spacing enlarged from 20.3 to 22.4 Å. The result can be attributed to the intercalation of N2200 into the out-of-plane lamella packing of PBDBT. The (010) peak of N2200 in PBDBT:N2200 film remains at q_z = 1.63 $Å^{-1}$. As the $PC_{71}BM$ concentration is increased, except the $PC_{71}BM$ scattering peak at q_{xy} = 1.33 $Å^{-1}$,[38] there is no apparent change in the scattering pattern, suggesting that the $PC_{71}BM$ filler do not significantly alter the molecular orientation of PBDBT and N2200. The coherence length (CL) of the (100) peak of PBDBT in each blend film was calculated using the Scherrer equation,[39−41] showing a monotonic increase from 43.1 Å (2:1:0) to 44.5 Å (2:1:0.1), 58.8 Å (2:1:0.5), and 66.3 Å (2:1:2), whereas that of the (010) peak of N2200 shows a monotonic decrease from 9.8 Å (2:1:0) to 9.4 Å (2:1:0.1), 8.3 Å (2:1:0.5), and 6.3 Å (2:1:2). The variation of CL suggests that the presence of $PC_{71}BM$ in the PBDBT:N2200 matrix promotes the growth of the PBDBT crystallite size but reduces the crystallization of the N2200 polymer chain. The increase of PBDBT crystallite size explains the obtained improvement in hole mobility. The reduced crystallization of N2200 polymer chain with increased $PC_{71}BM$ loading indicates the lowering of electron mobility. In fact, the electron mobility has the highest value at 2:1:0.5 blend, a result which infers that $PC_{71}BM$ plays a significant role in improving the electron mobility. A shoulder appears at q_{xy} = 1.33 $Å^{-1}$ due to the aggregation of $PC_{71}BM$[38] in the 2:1:0.5 blend, and it becomes apparent at the 2:1:2 blend.

From the optical perspective, the inclusion of $PC_{71}BM$ enhances the light absorption efficiency and the subsequent exciton quenching efficiency, and produces energy transfer effect. From the charge transport perspective, Figure 6 presents the schematic depictions of nanomorphology evolution of PBDBT:N2200 incorporating various amounts of $PC_{71}BM$ filler obtained from GIWAXS measurements. All blend films are composed of relatively pure crystalline phases of PBDBT and N2200 as well as amorphous phases. Several reports[38,42−44] have found that there is a critical concentration of fullerenes to be miscible with conjugated polymers, and above the critical content, fullerene aggregates begin to form resulting from demixing of fullerenes and polymers. Upon

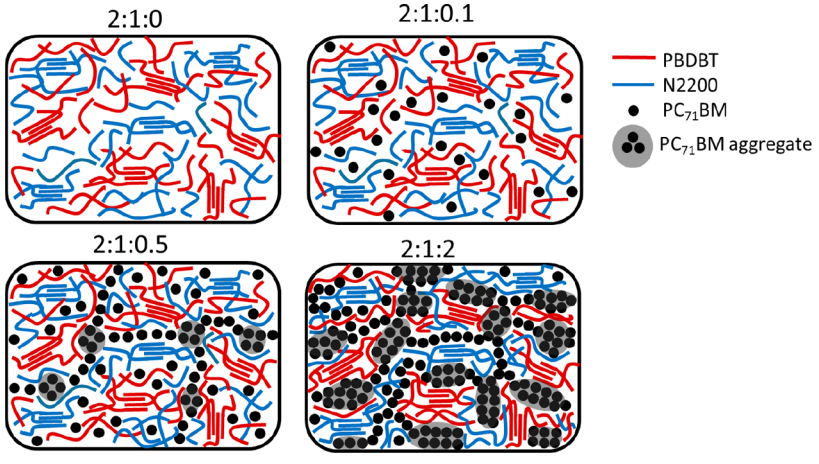

Figure 6. Schematics of PBDBT:N2200:$PC_{71}BM$ morphology at various weight ratios.

https://dx.doi.org/10.1021/acsaem.9b02302
ACS Appl. Energy Mater. 2020, 3, 4217−4225

adding a small amount of $PC_{71}BM$ (A_2/A_1 = 0.1), those fullerene molecules preferentially distribute in the amorphous phases of PBDBT and N2200, yielding molecularly mixed regions of polymers and fullerene. Those well dispersed $PC_{71}BM$ molecules in the amorphous region can facilitate exciton delocalization over neighboring molecules,[45−48] which promotes the exciton dissociation as evidenced by the PL quenching result and photocurrent analysis. Due to a very small amount of filler being added, we suspect that the added $PC_{71}BM$ molecules are insufficient to form percolation pathways in the molecularly mixed region to facilitate electron transport.[49] This is because that 2:1:0.1 blend carries similar electron mobility to the neat PBDBT:N2200 film though fullerene has higher electron mobility than N2200.[50,51] The enhanced J_{SC} of devices containing $PC_{71}BM$ is not mainly due to changes in charge transport ability. On the basis of our measurement, the emission of $PC_{71}BM$ strongly overlaps the absorption of N2200, which provides firm evidence to show that the improved J_{SC} at low $PC_{71}BM$ loading can be attributed to the energy transfer from $PC_{71}BM$ to N2200.

By further increasing the concentration of the filler, PL intensity of PBDBT is further quenched. At A_2/A_1 = 0.5, both the PL quenching and the exciton dissociation efficiency are maximized, suggesting the optimized D/A interface area created by PBDBT, N2200, and $PC_{71}BM$ in the blend. It is found that the blend carries the highest electron mobility, indicating that $PC_{71}BM$ is percolated and has significant contribution to electron transporting. As obtained, the charge transport is the most balanced and the interfacial charge recombination probability is minimized. Consequently, both optimal interface charge transport and balanced charge transport occur at 2:1:0.5 blend in conjunction with energy transfer effect; the largest improvement in J_{Sc} is thus obtained for highest PCE.

At high $PC_{71}BM$ loading (A_2/A_1 > 0.5), GIWAXS study yields a pronounced signal of $PC_{71}BM$ aggregates and TEM image shows a clear change of film morphology from fibrous to granular structure. Since more $PC_{71}BM$ aggregates demixed from the amorphous phase of PBDBT:N2200 blend, we suspect that those $PC_{71}BM$ aggregates could have interrupted most host donor−acceptor interactions; i.e., a replacement of most PBDBT-N2200 junctions by PBDBT−$PC_{71}BM$ ones. Thus, the PBDBT/N2200 interface area reduces and PBDBT/$PC_{71}BM$ (N2200/$PC_{71}BM$) contact surface increases. As a result, excitons generated in the $PC_{71}BM$ phase can have higher probability to be dissociated at the PBDBT/$PC_{71}BM$ junction, whereas those in the N2200 phase are less efficient to be split. Therefore, IPCE values from the response of N2200 decrease in the wavelength range of 650−800 nm, whereas those from $PC_{71}BM$ still increase in the wavelength shorter than 500 nm relative to that of the neat all-PSCs. In this stage, the charge transport in the blend becomes unbalanced due to the decreased electron mobility that originated from largely reduced N2200 crystallite size, which could be one of the reasons for the decreased J_{SC} at the high filler loading. Though the energy transfer effect is important, it may not have significant contribution to J_{SC} here because the PBDBT/N2200 surface area decreases and the charge transfer at N2200/$PC_{71}BM$ junctions is not efficient.

We note here that the vertical phase separation effect induced by including $PC_{71}BM$[50] may possibly occur in the studied system and affect the device performance. The schematic picture in Figure 6 depicts the spatial arrangement of donor and acceptor components within a limited depth range, which provides a scope for understanding the morphology evolution with the addition of $PC_{71}BM$.

We have tried to replace $PC_{71}BM$ with ITIC as acceptor filler without optimizing the best loading amount and also obtained an improved device performance, including higher PCE, strong PL quenching, and more balanced charge transport property (see Figure S6, Table S3). Since introducing acceptor filler into all-PSCs can effectively improve device performance, we then compare the storage and light-soaking stability of devices with and without optimal filler loading. For the storage stability, devices were stored in the dark in the laboratory environment and their performances were measured periodically. It is found that there is no appreciable difference in PCE values after 75 days. For the light-soaking stability, devices were continuously exposed to light irradiation at 100 mW/cm^2 from a calibrated solar simulator with AM 1.5 G filter in the laboratory environment for 135 min, and their performances were also evaluated periodically. As obtained, there is also negligible difference in the variation of PCE values after introducing filler into the neat all-PSCs. Therefore, the prescence of those fillers will not significantly affect both the storage stability and the light-soaking stability of devices (see Figure S7). In addition to stability, Yan et al.[51] have reported that the major factor hindering the device performance of all-PSCs is the germinate recombination of charges compared with polymer−fullerene systems. By using the concept of filler, the process can be effectively suppressed as revealed by the increased R_{rec}. Compared to conventional ternary devices based on PTB7-th:N2200:$PC_{71}BM$,[25] the electron mobility of our nonconventional ternary blend is improved at $PC_{71}BM$/N2200 = 0.5, whereas it is not the case for the conventional one up to $PC_{71}BM$/N2200 = 1 (50 wt % $PC_{71}BM$). The result indicates that less $PC_{71}BM$ amount in nonconventional ternary blend is sufficient to form percolation pathways between $PC_{71}BM$ domains to facilitate electron transport, an advantage of using the concept of filler.

4. CONCLUSION

We have successfully demonstrated a new concept of introducing small molecules as acceptors and also as fillers in all-PSCs to improve the device performance. The resulting filler-contained photoactive blend is a nonconventional ternary system in contrast to the conventional ternary system with overall fixed D/A ratio. A good filler for all-PSCs should be of good mobility, compatible with all-polymer blend and having the right energy band alignment with donor/acceptor polymer. Those selected acceptor fillers can homogeneouly distribute in the amorphous phase of an all-polymer matrix and efficiently improve exciton separation as well as geminate recombination. In addition, those filler molecules can also form a second transport pathway for electron traveling, which can effectively raise up the electron mobility. With an appropriate amount of filler, the charge transport in the nonconventional ternary blend becomes more balanced. As demonstrated, the optimal PCE value of 7.42% based on PBDBT:N2200:$PC_{71}BM$ blend is achievable and higher than the binary blend devices of PBDBT:N2200 and PBDBT:$PC_{71}BM$. Additionally, those filler-contained devices operate as stably as the neat all-PSCs. The proposed approach provides a design route for the development of mechanically stable and high performance solar cells.

https://dx.doi.org/10.1021/acsaem.9b02302
ACS Appl. Energy Mater. 2020, 3, 4217−4225

■ ASSOCIATED CONTENT

Supporting Information

The Supporting Information is available free of charge at https://pubs.acs.org/doi/10.1021/acsaem.9b02302.

Performances (Figures S1, S3, Table S1), PL spectra (Figure S2), $J_{ph}-V_{eff}$ analysis results (Table S2), mobility measurement by SCLC method (Figure S4), GIWAXS patterns (Figure S5), device study (Figure S6, Table S3), and stability comparison (Figure S7) (PDF)

■ AUTHOR INFORMATION

Corresponding Authors

Fang-Chi Hsu − *Department of Materials Science and Engineering, National United University, Miaoli 36003, Taiwan;* orcid.org/0000-0003-1961-5569; Email: fangchi@nuu.edu.tw

Yang-Fang Chen − *Department of Physics, National Taiwan University, Taipei 10617, Taiwan;* orcid.org/0000-0003-1203-5115; Email: yfchen@phys.ntu.edu.tw

Authors

Jin-Wen Luo − *Department of Materials Science and Engineering, National United University, Miaoli 36003, Taiwan*

Yu-Wei Su − *Department of Chemical Engineering, Feng-Chia University, Taichung 40724, Taiwan;* orcid.org/0000-0003-1303-7032

Cheng-Syun Yang − *Department of Materials Science and Engineering, National United University, Miaoli 36003, Taiwan*

Yu-An Lin − *Department of Materials Science and Engineering, National United University, Miaoli 36003, Taiwan*

Jia-Yu Lin − *Department of Physics, National Taiwan University, Taipei 10617, Taiwan*

Chi-Yuan Chang − *Department of Physics, National Taiwan University, Taipei 10617, Taiwan;* orcid.org/0000-0002-2033-1857

Chi-Ping Li − *Department of Chemical Engineering, National United University, Miaoli 36003, Taiwan*

Complete contact information is available at: https://pubs.acs.org/10.1021/acsaem.9b02302

Notes

The authors declare no competing financial interest.

■ ACKNOWLEDGMENTS

This work is supported by Ministry of Science and Technology, Taiwan (Project Nos. MOST 105-2112-M-239-001-MY3 and MOST 108-2112-M-239-002).

■ REFERENCES

(1) Yu, G.; Gao, J.; Hummelen, J. C.; Wudl, F.; Heeger, A. J. Polymer Photovoltaic Cells: Enhanced Efficiencies via a Network of Internal Donor-Acceptor Heterojunctions. *Science* **1995**, *270*, 1789−1791.

(2) Brabec, C. J.; Gowrisanker, S.; Halls, J. J.; Laird, D.; Jia, S.; Williams, S. P. Polymer−Fullerene Bulk-Heterojunction Solar Cells. *Adv. Mater.* **2010**, *22*, 3839−3856.

(3) Li, G.; Zhu, R.; Yang, Y. Polymer Solar Cells. *Nat. Photonics* **2012**, *6*, 153−161.

(4) Liang, Y. Z.; Xu, J.; Xia, S.; Tsai, T.; Wu, Y.; Li, G.; Ray, C.; Yu, L. For the Bright Future—Bulk Heterojunction Polymer Solar Cells with Power Conversion Efficiency of 7.4%. *Adv. Mater.* **2010**, *22*, E135−E138.

(5) Benten, H.; Mori, D.; Ohkita, H.; Ito, S. Recent Research Progress of Polymer Donor/Polymer Acceptor blend Solar Cells. *J. Mater. Chem. A* **2016**, *4*, 5340−5365.

(6) Li, Y.; Xu, G.; Cui, C.; Li, Y. Flexible and Semitransparent Organic Solar Cells. *Adv. Energy Mater.* **2018**, *8*, 1701791.

(7) Lee, W.; Jeong, S.; Lee, C.; Han, G.; Cho, C.; Lee, J.-Y.; Kim, B. J. Organic Photovoltaics: Self-Organization of Polymer Additive, Poly(2-vinylpyridine) via One-Step Solution Processing to Enhance the Efficiency and Stability of Polymer Solar Cells. *Adv. Energy Mater.* **2017**, *7*, 1602812.

(8) Wan, Q.; Guo, X.; Wang, Z.; Li, W.; Guo, B.; Ma, W.; Zhang, M.; Li, Y. 10.8% Efficiency Polymer Solar Cells Based on PTB7-Th and $PC_{71}BM$ via Binary Solvent Additives Treatment. *Adv. Funct. Mater.* **2016**, *26*, 6635−6640.

(9) Zhao, J.; Li, Y.; Yang, G.; Jiang, K.; Lin, H.; Ade, H.; Ma, W.; Yan, H. Efficient Organic Solar Cells Processed from Hydrocarbon Solvents. *Nat. Energy* **2016**, *1*, 15027.

(10) Kawashima, K.; Fukuhara, T.; Suda, Y.; Suzuki, Y.; Koganezawa, T.; Yoshida, H.; Ohkita, H.; Osaka, I.; Takimiya, K. Implication of Fluorine Atom on Electronic Properties, Ordering Structures, and Photovoltaic Performance in Naphthobisthiadiazole-Based Semiconducting Polymers. *J. Am. Chem. Soc.* **2016**, *138*, 10265−10275.

(11) Fan, B.; Ying, L.; Wang, Z.; He, B.; Jiang, X. − F.; Huang, F.; Cao, Y. Optimisation of Processing Solvent and Molecular Weight for the Production of Green-Solvent-Processed All-Polymer Solar Cells with Power Conversion Efficiency over 9%. *Energy Environ. Sci.* **2017**, *10*, 1243−1251.

(12) Fan, B.; Zhang, D.; Li, M.; Zhong, W.; Zeng, Z.; Ying, L.; Huang, F.; Cao, Y. Achieving Over 16% Efficiency for Single-Junction Organic Solar Cells. *Sci. China: Chem.* **2019**, *62*, 746−752.

(13) Ran, N. A.; Roland, S.; Love, J. A.; Savikhin, V.; Takacs, C. J.; Fu, Y. T.; Li, H.; Coropceanu, V.; Liu, X.; Brédas, J. L.; Bazan, G. C.; Toney, M. F.; Neher, D.; Nguyen, T.-Q. Impact of Interfacial Molecular Orientation on Radiative Recombination and Charge Generation Efficiency. *Nat. Commun.* **2017**, *8*, 79.

(14) Lee, J.; Singh, R.; Sin, D. H.; Kim, H. G.; Song, K. C.; Cho, K. A Nonfullerene Small Molecule Acceptor with 3D Interlocking Geometry Enabling Efficient Organic Solar Cells. *Adv. Mater.* **2016**, *28*, 69−76.

(15) Holliday, S.; Ashraf, R. S.; Wadsworth, A.; Baran, D.; Yousaf, S. A.; Nielsen, C. B.; Tan, C. H.; Dimitrov, S. D.; Shang, Z.; Gasparini, N.; Alamoudi, M.; Laquai, F.; Brabec, C. J.; Salleo, A.; Durrant, J. R.; McCulloch, I. High-Efficiency and Air-Stable P3HT-Based Polymer Solar Cells with a New Non-Fullerene Acceptor. *Nat. Commun.* **2016**, *7*, 11585.

(16) Jung, J. W.; Jo, J. W.; Chueh, C. C.; Liu, F.; Jo, W. H.; Russell, T. P.; Jen, A. K. Fluoro-Substituted N-Type Conjugated Polymers for Additive-Free All-Polymer Bulk Heterojunction Solar Cells with High Power Conversion Efficiency of 6.71%. *Adv. Mater.* **2015**, *27*, 3310−3317.

(17) Ye, L.; Jiao, X.; Zhou, M.; Zhang, S.; Yao, H.; Zhao, W.; Xia, A.; Ade, H.; Hou, J. Manipulating Aggregation and Molecular Orientation in All-Polymer Photovoltaic Cells. *Adv. Mater.* **2015**, *27*, 6046−6054.

(18) Kim, T.; Kim, J.-H.; Kang, T. E.; Lee, C.; Kang, H.; Shin, M.; Wang, C.; Ma, B.; Jeong, U.; Kim, T.-S.; Kim, B. J. Flexible, Highly Efficient All-Polymer Solar Cells. *Nat. Commun.* **2015**, *6*, 8547.

(19) Kim, T.; Choi, J.; Kim, H. J.; Lee, W.; Kim, B. J. Comparative Study of Thermal Stability, Morphology, and Performance of All-Polymer, Fullerene-Polymer, and Ternary Blend Solar Cells Based on the Same Polymer Donor. *Macromolecules* **2017**, *50*, 6861−6871.

(20) Fan, B.; Ying, L.; Zhu, P.; Pan, F.; Liu, F.; Chen, J.; Huang, F.; Cao, Y. All-Polymer Solar Cells Based on a Conjugated Polymer Containing Siloxane-Functionalized Side Chains with Efficiency over 10%. *Adv. Mater.* **2017**, *29*, 1703906.

(21) Li, Z.; Xu, X.; Zhang, W.; Meng, X.; Ma, W.; Yartsev, A.; Inganäs, O.; Andersson, M. R.; Janssen, R. A. J.; Wang, E. High Performance All-Polymer Solar Cells by Synergistic Effects of Fine-

Tuned Crystallinity and Solvent Annealing. *J. Am. Chem. Soc.* **2016**, *138*, 10935−10944.
(22) Ye, L.; Jiao, X.; Zhao, W.; Zhang, S.; Yao, H.; Li, S.; Ade, H.; Hou, J. Manipulation of Domain Purity and Orientational Ordering in High Performance All-Polymer Solar Cells. *Chem. Mater.* **2016**, *28*, 6178−6185.
(23) Xu, Y.; Yuan, J.; Sun, J.; Zhang, Y.; Ling, X.; Wu, H.; Zhang, G.; Chen, J.; Wang, Y.; Ma, W. Widely Applicable N-Type Molecular Doping for Enhanced Photovoltaic Performance of All-Polymer Solar Cells. *ACS Appl. Mater. Interfaces* **2018**, *10*, 2776−2784.
(24) Li, Z.; Xu, X.; Zhang, W.; Meng, X.; Genene, Z.; Ma, W.; Mammo, W.; Yartsev, A.; Andersson, M. R.; Janssen, R. A. J.; Wang, E. 9.0% Power Conversion Efficiency from Ternary All-Polymer Solar Cells. *Energy Environ. Sci.* **2017**, *10*, 2212−2221.
(25) Lee, W.; Kim, J. H.; Kim, T.; Kim, S.; Lee, C.; Kim, J. S.; Ahn, H.; Kim, T. S.; Kim, B. J. Mechanically Robust and High-Performance Ternary Solar Cells Combining the Merits of All-Polymer and Fullerene Blends. *J. Mater. Chem. A* **2018**, *6*, 4494−4503.
(26) Gao, L.; Zhang, Z.-G.; Xue, L.; Min, J.; Zhang, J.; Wei, Z.; Li, Y. All-polymer Solar Cells Based on Absorption-Complementary Polymer Donor and Acceptor with High Power Conversion Efficiency of 8.27%. *Adv. Mater.* **2016**, *28*, 1884−1890.
(27) Song, M.; Park, J. H.; Im, C. S.; Kim, D.-H.; Kang, Y. C.; Jin, S. H.; Jin, W. Y.; Kang, J. W. Highly Flexible and Transparent Conducting Silver Nanowire/ZnO Composite Film for Organic Solar Cells. *Nano Res.* **2014**, *7*, 1370−1379.
(28) Zhang, X.; Zuo, X.; Xie, S.; Yuan, J.; Zhou, H.; Zhang, Y. Understanding Charge Transport and Recombination Losses in High Performance Polymer Solar Cells with Non-Fullerene Acceptors. *J. Mater. Chem. A* **2017**, *5*, 17230−17239.
(29) Xu, Y.; Yuan, J.; Sun, J.; Zhang, Y.; Ling, X.; Wu, H.; Zhang, G.; Chen, J.; Wang, Y.; Ma, W. Widely Applicable N-Type Molecular Doping for Enhanced Photovoltaic Performance of All-Polymer Solar Cells. *ACS Appl. Mater. Interfaces* **2018**, *10*, 2776−2784.
(30) Lu, L. Y.; Xu, T.; Chen, W.; Landry, E. S.; Yu, L. Ternary Blend Polymer Solar Cells with Enhanced Power Conversion Efficiency. *Nat. Photonics* **2014**, *8*, 716−722.
(31) Hao, Y.; Song, J.; Yang, F.; Hao, Y.; Sun, Q.; Guo, J.; Cui, Y.; Wang, H.; Zhu, F. Improved Performance of Organic Solar Cells by Incorporating Silica-coated Silver Nanoparticles in the Buffer Layer. *J. Mater. Chem. C* **2015**, *3*, 1082.
(32) Shrotriya, V.; Wu, E. H.-E.; Li, G.; Yao, Y.; Yang, Y. Efficient Light Harvesting in Multiple-Device Stacked Structure for Polymer Solar Cells. *Appl. Phys. Lett.* **2006**, *88*, 064104.
(33) Zhang, Y.; Xu, Y.; Ford, M. J.; Li, F.; Sun, J.; Ling, X.; Wang, Y.; Gu, J.; Yuan, J.; Ma, W. Thermally Stable All-Polymer Solar Cells with High Tolerance on Blend Ratio. *Adv. Energy Mater.* **2018**, *8*, 1800029.
(34) Bisquert, J. Theory of the Impedance of Electron Diffusion and Recombination in a Thin Layer. *J. Phys. Chem. B* **2002**, *106*, 325−333.
(35) Yuan, J.; Guo, W.; Xia, Y.; Ford, M. J.; Jin, F.; Liu, D.; Zhao, H.; Inganäs, O.; Bazan, G. C.; Ma, W. Comparing the Device Physics, Dynamics and Morphology of Polymer Solar Cells Employing Conventional PCBM and Non-Fullerene Polymer Acceptor N2200. *Nano Energy* **2017**, *35*, 251−262.
(36) Yuan, J.; Ford, M. J.; Zhang, Y.; Dong, H.; Li, Z.; Li, Y.; Nguyen, T. − Q.; Bazan, G. C.; Ma, W. Toward Thermal Stable and High Photovoltaic Efficiency Ternary Conjugated Copolymers: Influence of Backbone Fluorination and Regioselectivity. *Chem. Mater.* **2017**, *29*, 1758−1768.
(37) Huang, W.; Chandrasekaran, N.; Prasad, S. K. K.; Gann, E.; Thomsen, L.; Kabra, D.; Hodgkiss, J. M.; Cheng, Y.-B.; McNeill, C. R. Impact of Fullerene Mixing Behavior on the Microstructure, Photophysics, and Device Performance of Polymer/Fullerene Solar Cells. *ACS Appl. Mater. Interfaces* **2016**, *8*, 29608−29618.
(38) Kim, K.-H.; Park, S.; Yu, H.; Kang, H.; Song, I.; Oh, J. H.; Kim, B. J. Determining Optimal Crystallinity of Diketopyrrolopyrrole-Based Terpolymers for Highly Efficient Polymer Solar Cells and Transistors. *Chem. Mater.* **2014**, *26*, 6963−6970.
(39) Huang, Y.; Kramer, E. J.; Heeger, A. J.; Bazan, G. C. Bulk Heterojunction Solar Cells: Morphology and Performance Relationships. *Chem. Rev.* **2014**, *114*, 7006−7043.
(40) Rivnay, J.; Mannsfeld, S. C. B.; Miller, C. E.; Salleo, A.; Toney, M. F. Quantitative Determination of Organic Semiconductor Microstructure from the Molecular to Device Scale. *Chem. Rev.* **2012**, *112*, 5488−5519.
(41) Bartelt, J. A.; Beiley, Z. M.; Hoke, E. T.; Mateker, W. R.; Douglas, J. D.; Collins, B. A.; Tumbleston, J. R.; Graham, K. R.; Amassian, A.; Ade, H.; Fréchet, J. M. J.; Toney, M. F.; McGehee, M. D. The Importance of Fullerene Percolation in the Mixed Regions of Polymer−Fullerene Bulk Heterojunction Solar Cells. *Adv. Energy Mater.* **2013**, *3*, 364−374.
(42) Collins, B. A.; Li, Z.; McNeill, C. R.; Ade, H. Fullerene-Dependent Miscibility in the Silole-Containing Copolymer PSBTBT-08. *Macromolecules* **2011**, *44*, 9747−9751.
(43) Chen, H.; Peet, J.; Hu, S.; Azoulay, J.; Bazan, G.; Dadmun, M. The Role of Fullerene Mixing Behavior in the Performance of Organic Photovoltaics: PCBM in Low-Bandgap Polymers. *Adv. Funct. Mater.* **2014**, *24*, 140−150.
(44) Schubert, M.; Collins, B. A.; Mangold, H.; Howard, I. A.; Schindler, W.; Vandewal, K.; Roland, S.; Behrends, J.; Kraffert, F.; Steyrleuthner, R.; Chen, Z.; Fostiropoulos, K.; Bittl, R.; Salleo, A.; Facchetti, A.; Laquai, F.; Ade, H. W.; Neher, D. Correlated Donor/Acceptor Crystal Orientation Controls Photocurrent Generation in All-Polymer Solar Cells. *Adv. Funct. Mater.* **2014**, *24*, 4068−4081.
(45) Caruso, D.; Troisi, A. Long-Range Exciton Dissociation in Organic Solar Cells. *Proc. Natl. Acad. Sci. U. S. A.* **2012**, *109*, 13498−13502.
(46) Gregg, B. A. Entropy of Charge Separation in Organic Photovoltaic Cells: The Benefit of Higher Dimensionality. *J. Phys. Chem. Lett.* **2011**, *2*, 3013−3015.
(47) McMahon, D. P.; Cheung, D. L.; Troisi, A. Why Holes and Electrons Separate So Well in Polymer/Fullerene Photovoltaic Cells. *J. Phys. Chem. Lett.* **2011**, *2*, 2737−2741.
(48) Kesava, S. V.; Fei, Z.; Rimshaw, A. D.; Wang, C.; Hexemer, A.; Asbury, J. B.; Heeney, M.; Gomez, E. D. Domain Compositions and Fullerene Aggregation Govern Charge Photogeneration in Polymer/Fullerene Solar Cells. *Adv. Energy Mater.* **2014**, *4*, 1400116.
(49) Yuan, J.; Guo, W.; Xia, Y.; Ford, M. J.; Jin, F.; Liu, D.; Zhao, H.; Inganas, O.; Bazan, G. C.; Ma, W. Comparing the Device Physics, Dynamics, and Morphology of Polymer Solar Cells Employing Conventional PCBM and Non-Fullerene Polymer Acceptor N2200. *Nano Energy* **2017**, *35*, 251−262.
(50) Bi, P.; Xiao, T.; Yang, X.; Niu, M.; Wen, Z.; Zhang, K.; Qin, W.; So, S. K.; Lu, G.; Hao, X.; Liu, H. Regulating the Vertical Phase Distribution by Fullerene-Derivative in High Performance Ternary Organic Solar Cells. *Nano Energy* **2018**, *46*, 81−90.
(51) Zhu, Z.; Chueh, C.-C.; Zhang, G.; Huang, F.; Yan, H.; Jen, A. K. Y. Improved Ambient-Stable Perovskite Solar Cells Enhanced by a Hybrid Polymeric Electron-Transporting Layer. *ChemSusChem* **2016**, *9*, 2586−2591.

https://dx.doi.org/10.1021/acsaem.9b02302
ACS Appl. Energy Mater. 2020, 3, 4217−4225